30TH INTERNATIONAL COSMIC RAY CONFERENCE

Particle acceleration by multiple parallel shocks

JONI TAMMI & PAUL DEMPSEY
UCD School of Mathematical Sciences, University College Dublin, Belfield, Dublin 4, Ireland.
joni.tammi@iki.fi, paul.dempsey@ucd.ie

Abstract: We present both numerical and semi-analytical results on test-particle acceleration in multiple parallel shocks. We apply a kinetic Monte Carlo code and an eigenfunction expansion method to calculate the distribution functions for electron populations accelerated in subsequent parallel shocks with speeds ranging from non- to fully-relativistic. We examine the levels of particle anisotropy at the shocks and discuss the implications for AGN and microquasar jets.

Introduction

Fermi acceleration at multiple non-relativistic shocks has been dealt with in detail by [8] and [10]. However, many objects that are likely to contain multiple shocks are relativistic, e.g., the jets of active galactic nuclei (AGNi), [11] the internal shock models of microquasars [6] and both the internal shock and reverse shock models of gamma ray bursts. [4,9] While the external shocks in these sources are inevitably strong, internal shocks can be weak, [4,6] either due to hydrodynamic pressure in parallel shocks or magnetohydrodynamic pressure in perpendicular shocks. Strong relativistic shocks are known to be capable of producing hard particle spectra with $N(E) \propto E^{-2.2}$ via the first-order Fermi mechanism. On the other hand the first-order mechanism produces much softer spectra with weak shocks. [7] However, in the case of a pre-existing hard power law population of particles then either inclusion of the shock drift mechanism [1] or small-angle diffusion [3] leads to an amplification of this power law far above that expected from purely adiabatic compression.

In this paper we consider hard power law spectra,

$$N(E) \propto E^{-\sigma},$$

created at a strong shock by the first-order acceleration mechanism, which are swept up by a weak shock. There is a number of physical scenarios in which this is possible; one such possibility is in microquasars and the parsec-scale jets of AGNi where electrons accelerated at an external shock are advected downstream of it towards the following internal shocks. Another scenario is the collision of two expanding shells of plasma where the weak reverse shock of the first shell sweeps up the high energy electrons produced by strong forward shock of the second shell.

In this paper we restrict ourselves to mildly relativistic external shocks, applicable to most AGNi and microquasars. However, the internal shocks of these sources can still have high Lorentz factors due to outbursts of the central engine.

Methods

The semi-analytic eigenfunction approach is based on solving the steady-state particle transport equation for the phase space distribution function:

$$\Gamma(u+\mu)\frac{\partial f}{\partial z} = \frac{\partial}{\partial \mu} D_{\mu\mu} \frac{\partial f}{\partial \mu},$$

where u is the bulk flow speed in the shock rest frame, $\Gamma = (1-u^2)^{-1/2}$, μ is the pitch-angle and $D_{\mu\mu}$ is the pitch-angle diffusion coefficient. This equation holds separately upstream and downstream of the shock, and boundary conditions are required to find the full solution. One condition is that the distributions match at the shock front, i.e., $f_-(p_-, \mu_-, 0) = f_+(p_+, \mu_+, 0)$, where the plus/minus sign denotes quantities upstream/downstream of the shock. We also require

Prof	$v_{\rm sh1}$	$v_{\rm do1}$	r_1	$v_{\rm sh2}$	$v_{\rm do2}$
A	.3000	.2293	3.95	.7290	.61933
B	.7070	.5965	3.70	.9770	.95731
C	.9500	.9105	3.25	.9989	.99783
D	.9800	.9619	3.10	.9997	.99934

Table 1: The sets used. The speed for the both shocks, $v_{\rm sh1}$ and $v_{\rm sh2}$, and the corresponding downstream flow speeds, $v_{\rm do1}$ and $v_{\rm do2}$, and the compression ratio of the first shocks, r_1, are given in the far upstream rest frame (observer's frame); all calculations and simulations are carried out in the relevant shock rest frames. Compression ratio of the second shock is 3 in all cases.

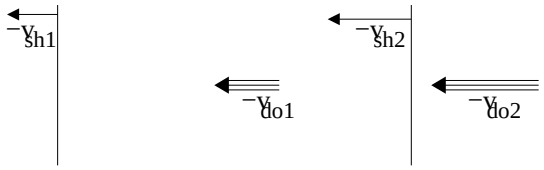

Figure 1: Simple model of the flow profile considered in this paper. The shocks are far enough apart that particles once a particle crossed the second shock it can never return to the first shock.

the distribution to be bounded infinitely far downstream. The distribution must be given far upstream and it is zero when only injection at the shock is considered. We can expand f as

$$f(p,\mu,z) = \sum_{i=-\infty}^{\infty} a_i(p) Q_i(\mu) \exp\left(\Lambda_i z/\Gamma\right)$$

where $(Q_i(\mu), \Lambda_i)$ are eigenfunction–eigenvalue pairs satisfying

$$\frac{d}{d\mu} D_{\mu\mu} \frac{dQ_i}{d\mu} = \Lambda_i (u+\mu) Q_i.$$

If the far upstream distribution is $g(p_-)$, then the boundary conditions imply

$$g(p_-) + \sum_{i>0} a_i^-(p_-) Q_i^-(\mu_-) = \sum_{i\le 0} a_i^+(p_+) Q_i^+(\mu_+).$$

If the far upstream distribution follows a power law with index s_1, i.e., $g(p_-) = A_0 p_-^{-s_1}$, we can find solutions with $a_i^\pm(p_\pm) = a_i^\pm p_\pm^{-s_1}$ by multiplying the matching condition by $Q_j^+(u_+ + \mu_+)$ and integrating over μ_+ for $j > 0$. The same applies also if we one considers only monoenergetic injection at the shock. In this case, letting

$$W_{i,j} = \int_{-1}^{1} (1 + u_{\rm rel}\mu_-)^{s_1} (u_+ + \mu_+) \times Q_j^+(\mu_+) Q_j^-(\mu_-)\, d\mu_+,$$

s_1 is found by the condition $\det \mathbf{W} = 0$ as in [7].

We also used a kinetic Monte Carlo test-particle simulation[1] for comparison. We injected particles in the upstream of a one-dimensional step shock, and followed them under the guiding-centre approximation until they reach a pre-defined escape boundary. This boundary was set sufficiently far away in the downstream to make sure the particles have reached isotropy in the downstream plasma frame. When a particle crossed the boundary, it was either "absorbed to the downstream", i.e., removed from the simulation, or mirrored mimicking the case of the particle recrossing the shock after returning from far downstream. This was done with the help of the probability of return (see, e.g., [5]). Also particle splitting was used to improve statistics: when a particle reached certain energy, it was replaced by two "daughter particles", which were otherwise identical to their "mother", but had only half of the original statistical weight.

In the simulation particles were scattered at the end of each Monte Carlo time-step. The small-angle scatterings are elastic in the rest frame of the scattering centres, which are taken to be moving with the local flow speed, so the energy remains unchanged over a scattering in the local flow frame. Energy losses were omitted in these simulations to allow for better comparison with the semi-analytical results.

For the first shock the injected particles have a small initial energy and random direction. For the second shock we inject the particles accelerated in the first shock. The particle properties were measured in the local plasma frame, so the downstream properties for the first shock simply become upstream properties for the second. However, the the shocks in each case (see Table 1) were simulated separately, so for example particles escaping upstream from the second shock cannot travel back to the first shock.

1. `http://www.iki.fi/joni.tammi/qshock`

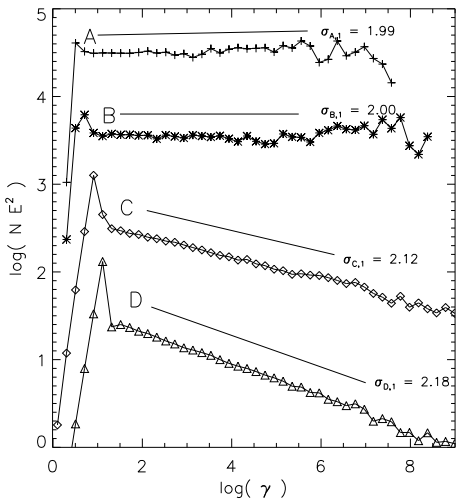

Figure 2: Simulated energy spectra (multiplied by E^2) downstream of the first shocks for the profiles given in Table 1. Spectra have been shifted vertically to allow for better comparison. Solid lines give slopes obtained from the eigenfunction method.

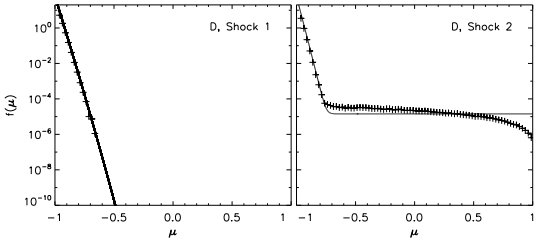

Figure 3: Distribution of power-law tail particles at both D-profile shocks as measured in the upstream rest frame.

Results and Discussion

As outlined in the introduction the process we are interested in the process where a power-law distribution, pre-created at a strong shock, is being swept and further accelerated by a weak shock. We consider four different velocity profiles (see Figure 1 and Table 1), for which the compression ratio of the first shock is calculated from the hydrodynamical jump conditions for a plasma satisfying the Jüttner-Synge equation of state. The compression ratio of the second shock is 3 in all cases.

Energy spectra and pitch-angle distributions were obtained using both the eigenfunction method and particle simulations, and there is good agreement between the two methods. Figure 2 shows the energy spectra a few scattering lengths downstream of the first shock for all profiles together with the semi-analytically obtained spectral slopes. While the pitch-angle distribution is isotropic at this distance downstream, it can be highly anisotropic at the shock front.[2] This can be seen in Figure 3, showing the pitch-angle distribution at the both shocks for profile D, as measured in the corresponding upstream rest frame.

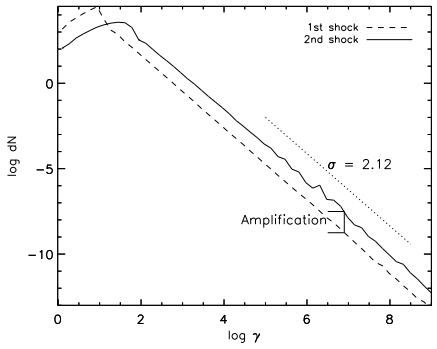

Figure 4: Particle spectra before (dashed line) and after the second shock (solid line), as measured in the local plasma frame, for the C case. The dotted line shows the slope obtained from the eigenfunction method.

The spectral index doesn't change at the second shock crossing due to the fact the the "natural spectral index" of such a weak shock is greater than the index for the injected spectra. The power-law is shifted due to the Lorentz transformation across the shock, and additionally due to the further acceleration by the first-order process. The compression of the plasma at the shock crossing doesn't affect the plain energy spectrum, but needs to be taken into account when comparing the distribution functions. In addition to compression and the change of frames across the shock, the shock acceleration mechanism can lead to significant additional amplification. Example is shown in Fig. 4, where the number of the power-law particles at a given energy (in the local plasma frame) is increased by the

2. This poses difficulties for comparing the μ distribution in the upstream, as for a relativistic shock (cf. case D) one would need to simulate of the order of 10^{90} crossings to get one crossing with $\mu = +1$ due to the extreme anisotropy. For this reason, the data for simulated particles does not extend far from $\mu' = -1$ in this frame.

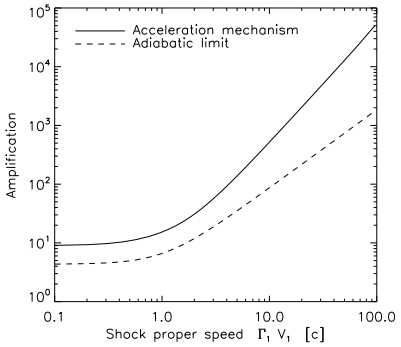

Figure 5: Amplification of spectrum as a function of shock proper speed. See text for details.

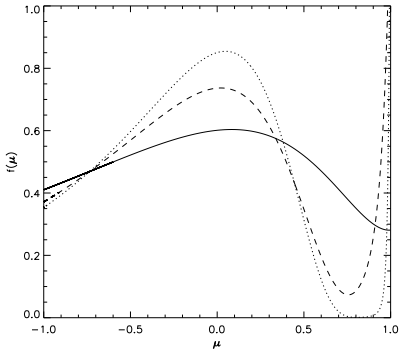

Figure 6: Pitch-angle distribution, as measured in the downstream frame, of the particles for cases A (solid line), B, (dashed) and D (dotted) for the second shock.

factor of 17.4 (case C), and general behaviour of the amplification with respect to the shock speed is drawn for an example case (spectral index $\sigma = 2$ and compression ratio $r = 3$) in Fig. 5.

The peak near $\mu = +1$ in the particle pitch-angle distribution at the shock measured in the downstream rest frame is due to particles that cross the shock and never return. For the first shock these particles are not considered as they are not in the power-law part of the spectrum; in the second shock, however, these are well beyond the thermal population and thus may have some signifigance e.g. in radiation modelling, as the highest-energy particles can radiate their energy away before they have had time to isotropise in the downstream of the second shock. As expected, Figure 6 shows that this proportion increases as the shock becomes relativistic.

The eigenfunction method and test-particle simulations broadly agree on the level of amplification. However, the eigenfunction method has no cut-offs in particle energy due to assumptions about energy losses. The simulations show that as well as an amplification in the magnitude of the power law part of the distribution, the power law extends to a higher cut-off energy. This will result in a higher peak energy in the synchrotron spectra behind the shock than what exists ahead of the second shock.

While this paper restricts itself to weak subsequent shocks, future work will use both presented methods to examine re-accleration at strong shocks in order to produce results comparible to [8] and [10] in the relativistic limit.

In addition to energy losses due to, e.g., synchrotron emission or adiabatic expansion, the current study omits possible effects due to turbulence transmission (see Tammi, elsewhere in this volume), second-order acceleration between the shocks [12], as well as injection of new low-energy particles into the second shock.

References

[1] Begelman, M. C., & Kirk, J. G. 1990, ApJ, 353, 66
[2] Bicknell, G. V., & Begelman, M. C. 1996, ApJ, 467, 597
[3] Dempsey, P., & Duffy, P. 2007, Ap&SS, 309, 167
[4] Fan, Y. Z., Wei, D. M., & Zhang, B. 2004, MNRAS, 354, 1031
[5] Jones, F. C. & Ellison, D. C. 1991, Space Sci. Rev., 58, 259
[6] Kaiser, C. R., Sunyaev, R., & Spruit, H. C. 2000, A&A, 356, 975
[7] Kirk, J. G., Guthmann, A. W., Gallant, Y. A., & Achterberg, A. 2000, ApJ, 542, 235
[8] Melrose, D. B., & Pope, M. H. 1993, PASAu, 10, 222
[9] Mészáros, P., & Rees, M. J. 1999, MNRAS, 306, L39
[10] Pope, M. H., & Melrose, D. B. 1994, PASAu, 11, 175
[11] Rees, M. J. 1978, MNRAS, 184, 61P
[12] Virtanen, J. J. P, & Vainio, R. 2005, ApJ, 621, 313